Chapter 12
Cellular spacing: analysis and modelling of retinal mosaics

Stephen J. Eglen

Abstract A key step in nervous system development is the spatial positioning of neurons within a structure. In this chapter I review the mechanisms by which the cellular spacing of neuronal networks emerges. In particular, I focus on the spatial distribution of neurons within the retina. The retina is ideal for studying such developmental mechanisms because of its multilayered structure and specific neurochemical markers can reliably label all neurons of a given type. This chapter describes the quantitative methods used for assessing spatial regularity of neuronal distributions and computational methods for simulating these distributions.

12.1 Introduction

The retina is a relatively small neural structure located at the back of the eye. It is a multilayered structure (Figure 12.1): photoreceptors toward the back of the eye convert light into neural activity which then propagates through several layers where it is modulated by lateral connections (via horizontal and amacrine cells) until reaching the ganglion cell layer. Retinal ganglion cells (RGCs) encode the visual scene into spike trains which then leave along the optic nerve and into the brain for further processing. For a general overview of retinal processing, see Wässle (2004).

The layered organisation of the retina makes for relatively easy identification of cell type, as each cell type tends to occur in only one layer of the retina. Taking a cross section through one of the layers, such as the ganglion cell layer, reveals a further aspect of structural organisation within the retina. Cells of a given type are positioned semi-regularly through a layer, forming what is commonly termed a retinal mosaic, due to the way that the cell bodies and their dendrites tile the sur-

Stephen J. Eglen
Cambridge Computational Biology Institute, University of Cambridge e-mail: sje30@cam.ac.uk
Citation: Eglen, SJ (2012). Cellular spacing: analysis and modelling of retinal mosaics. In Le Novére, N, ed., Computational Systems Neurobiology, chapter 12. Springer, pages 365–385.

face (Figure 12.2). (For the rest of this article, when I refer to retinal mosaics, it will mostly refer to the positioning of the cell body, assuming that the surrounding dendritic arbor is also tiled. For further details on modelling dendritic growth, see Chapter 13.) Most cell types form independent mosaics (see later for a rigorous definition of independence), such that the presence of a retinal mosaic is often used to determine whether a given population forms an independent type (Cook, 1998). Together with reliable biochemical markers for reliably staining individual cell types, this has meant the catalogue of cell types (five classes, divided into about 60 types, depending on species) within the retina is nearing completion (Masland, 2004).

What function might such retinal mosaics perform? For photoreceptors, having a regular spacing of neurons is presumably necessary to sample the entire visual field, avoiding any 'blind spots'. However, the spatial distribution of photoreceptors is slightly different to that of other cell types as they tend to be tightly packed against each other (Figure 12.3). Short wavelength cones ('blue cones') tend to be regularly spaced, as they are relatively sparse compared to the medium/long wavelength cones, which are randomly arranged (Roorda et al, 2001). However, in other layers of the retina, after sampling of the visual world, the advantages of a regular mosaic are not so obvious. One hypothesis is that regular arrangements of individual cell types in different layers may aid in the developmental wiring of connections between cell types (Galli-Resta, 2002). Chapter 14 discusses the wiring of connections between neurons.) However, this wiring hypothesis has yet to be explored.

In this chapter I will describe the quantitative methods for the analysis and modelling of retinal mosaics, with an aim to understanding the developmental mechanisms that can generate such regular distributions of neurons. Although this work focuses on retinal neurons, it is hoped that similar principles apply to other parts of the CNS. Whether regular distributions of neurons exist or not in other parts of the CNS is still unclear, due to the larger number of cell types in other regions, and the lack of reliable markers for staining individual cell types early in development (Cook and Chalupa, 2000).

12.2 Quantifying regularity

Several methods have been developed for the quantification of the spatial distribution of retinal neurons. In this section, I briefly outline the main methods employed. The methods will be demonstrated on an example data set, shown in Figure 12.4.

12.2.1 Regularity index

The most popular method for quantifying mosaic measures is the regularity index (Wässle and Riemann, 1978). For each neuron in the field, the distance to the nearest-neighbouring neuron is measured and plotted in a histogram. The regularity

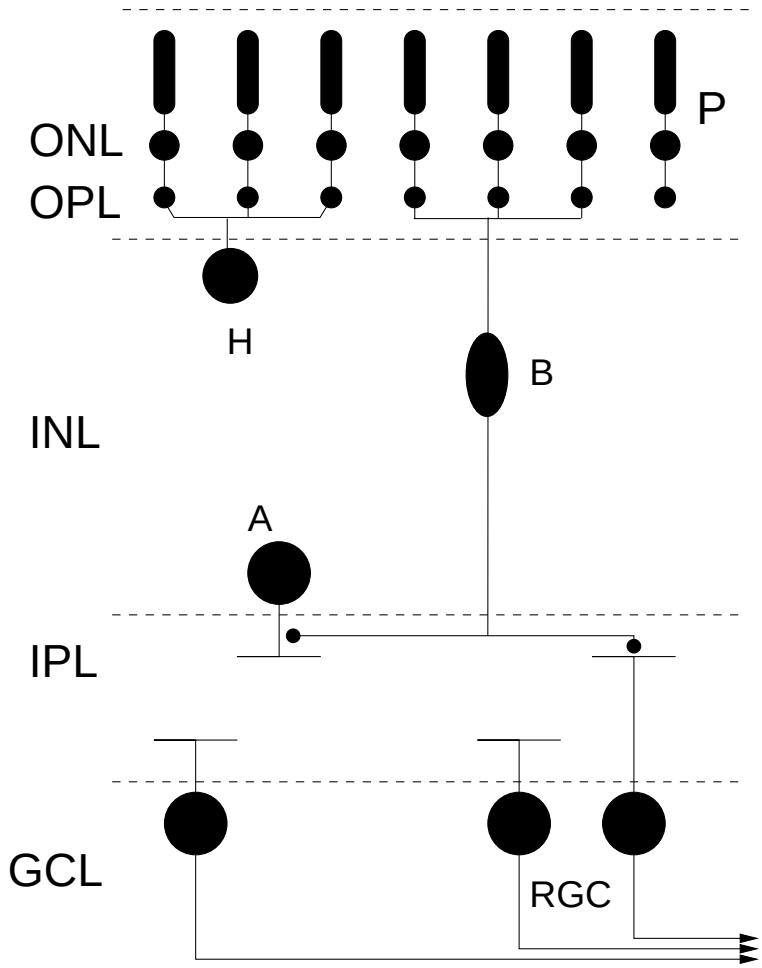

Fig. 12.1 Cross-section of a vertebrate retina. The retina is organised into three cell-dense layers (ONL: outer nuclear layer, INL: inner nuclear layer, GCL: ganglion cell layer). Connections between layers are predominantly made in the OPL (outer plexiform layer) and IPL (inner plexiform layer). Each of these layers can be regarded as a two-dimensional sheet. There are five major classes of retinal neuron: photoreceptors (P), horizontal cells (H), bipolar cells (B), amacrine cells (A) and retinal ganglion cells (RGC). Photoreceptors transduce light into neural activity, which then propagates to the RGCs via the bipolar cells. Both the horizontal and amacrine cells have widespread lateral interactions that modulate neural activity. Finally, axons of the RGCs form the optic nerve, carrying the neural signal from the eye to the brain for further processing. Cells of a particular class are usually restricted to a given layer within the retina, allowing for easier identification of individual cell classes. The spatial location of all neurons within a layer can then be revealed using various staining techniques (see Figures 12.2,12.3).

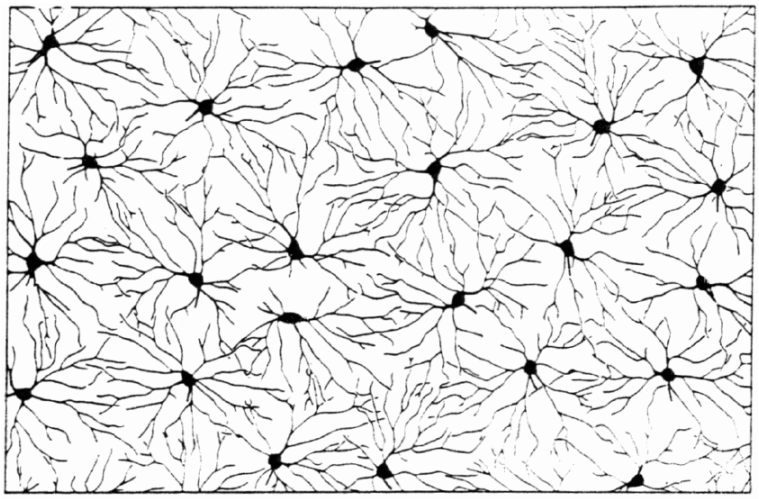

Fig. 12.2 Regular arrangement of on-centre alpha retinal ganglion cells from cat retina. The area shown is approximately 1.7×1.2 mm. The dendrites around each cell body tile the retinal surface, and the cell bodies seem roughly equally-spaced from each other. In this article, 'field' means the area of tissue within which the neurons are observed. Other neurons (e.g. off-centre alpha retinal ganglion cells) within the same layer are not shown. Reproduced by permission from Macmillan Publishers Ltd: Nature **292:**344–345, copyright 1981.

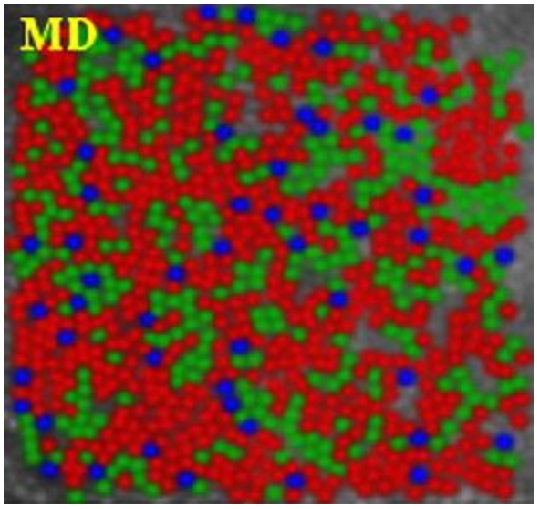

Fig. 12.3 Close packing of cone photoreceptors in a human retina (subject named MD). The three different classes of photoreceptor are coloured blue (short wavelength), green (medium wavelength) and red (long wavelength). Approximate width of view: 20 arc min. Reproduced from (Hofer et al, 2005) with permission of the Society for Neuroscience.

index (RI) is simply the mean of this distribution divided by its standard deviation. For the example in Figure 12.4, the RI of 5.1 indicates a highly regular mosaic.

Calculating a measure such as this immediately raises the question of how to interpret this number. Cook (1996) first investigated the properties of the RI (termed the conformity ratio in his article). The baseline to compare against is when the neurons are placed at random throughout the field — this is termed complete spatial randomness (CSR). The RI for neurons arranged randomly is 1.9, and the more regular the arrangement, the higher the RI. For retinal mosaics observed to date, the RI is typically 3–8. However, the exact threshold for determining whether the mosaic is non-randomly arranged depends on the number of neurons and the geometry of the field (Cook, 1996). Furthermore, the physical size of the soma may introduce lower limits onto the size of the nearest-neighbour distances. However, all of these can be handled appropriately by using Monte-Carlo techniques, see later.

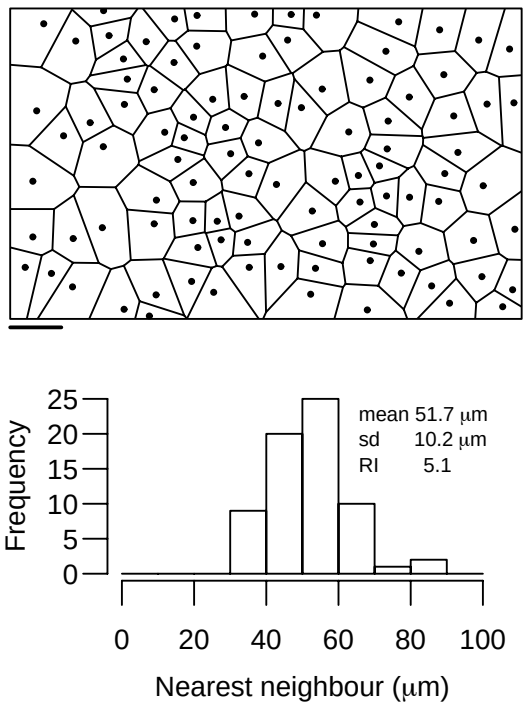

Fig. 12.4 Example mosaic (synthetic data set). Neurons are drawn as circles with 10 μm diameter representing typical soma size; scale bar: 100 μm. Each neuron is surrounded by its Voronoi polygon, showing the region of space closest to that point. The histogram underneath shows the distribution of nearest-neighbour distances, along with the regularity index (RI) of 5.1. This RI is typical of regular mosaics, such as cholinergic amacrine neurons.

12.2.2 Autocorrelation methods

A key limitation of the RI measure is that it is based only on the distribution of distances to nearest-neighbours. Autocorrelation-based methods are more powerful as they include the relative distance of all points, not just the nearest-neighbour. Such autocorrelation methods were made popular in the retinal mosaic literature by Rodieck (1991), although these methods were introduced much earlier in the spatial statistics literature (Ripley, 1976). An autocorrelation plot is created by taking one cell as the reference neuron, and plotting the relative position of all other neurons in a plot. This is repeated using each neuron as a reference neuron to build up the autocorrelation plot shown in Figure 12.5A. Annuli are drawn 10 μm apart, and clearly show a 'exclusion zone' effect: no two neurons are closer than about 40 μm apart, but beyond this distance, there is no further structure to the plot. This indicates that neurons perhaps are operating under the rule that they simply should avoid becoming 'too close' to each other, but there are no further constraints imposed.

Within each annulus of the autocorrelation plot, there is rarely little spatial variation. Each annulus can thus concisely be described by one number, the density of points in that annulus. The density of each annulus then forms the density recovery profile (DRP; Figure 12.5B) which is the usual way of summarising the autocorrelation. Again this clearly shows the exclusion zone principle acting up to around 40 μm, and beyond that the density of each annulus fluctuates around the mean density (horizontal line). Further quantification of the DRP is possible; for example, the size of the exclusion zone can be quantified by the effective radius shown in the figure as a vertical line; see (Rodieck, 1991) for further details. The DRP and its associated statistics are useful complements to the nearest-neighbour methods.

One limitation of the DRP approach is that the results may be dependent on the size of each annulus: smaller annuli should lead to more sensitive estimation of DRP parameters such as the effective radius. However with smaller annuli, the neuronal counts within each annulus can be quite small and thus the density estimates may vary significantly. Cumulative histograms of counts are more robust, by avoiding bin sizes, and have been proposed in spatial statistics (Ripley, 1976; Diggle, 2002). In particular, Ripley's K function is effectively the integral of the DRP. The K function is defined as:

$$K(t) = \frac{|A|}{n(n-1)} \sum_{i=1}^{n} \sum_{j \neq i} w(i,j)^{-1} I(||\mathbf{x}_i - \mathbf{x}_j|| \leq t) \tag{12.1}$$

In this function, $\mathbf{x}_i$ is a 2-d vector representing the position of neuron i; hence $I(\cdot)$ counts how many pairs of neuron are less than or equal to some distance t apart. $|A|$ is the field area, and n is the number of neurons. The term $w(i,j)$ is a weighting factor to correct for border effects, as described in the next section (Diggle, 2002). Under the null hypothesis of CSR, the theoretical K function is $K(t) = \pi t^2$. Finally, $L(t) = (K(t)/\pi)^{0.5}$ is used for plotting purposes.

Figure 12.5C shows the L function corresponding to the DRP in panel B. The null hypothesis of CSR is given by $L(t) = t$, shown in the dotted line, and deviations of

$L(t)$ below that line indicate regularity, as is the case here. ($L(t) > t$ would indicate that the neurons are clustered, rather than spaced-apart.)

Many other statistics are also available, including Voronoi-based measures, as well as other cumulative distance functions from the spatial statistics literature (notably the F and G functions); for further details, see (Diggle, 2002). It is an open question as to which of these functions are most useful for discriminating patterns, hence it is good practice to compare the effectiveness of several functions.

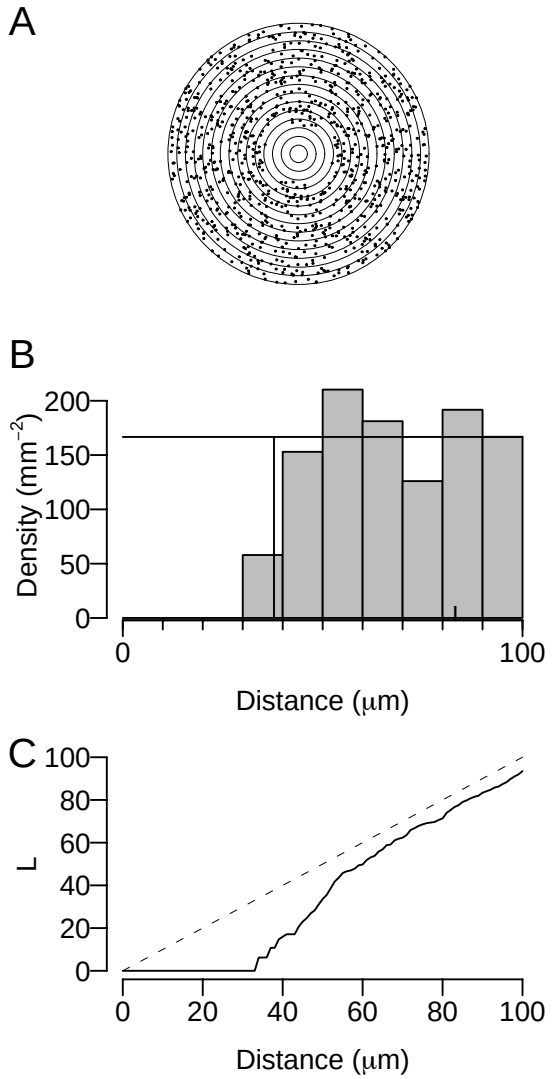

Fig. 12.5 Autocorrelation-based analysis of the mosaic shown in Figure 12.4. A: autocorrelation plot. Each dot represents the position of a cell relative to another neuron in the field. Annuli are spaced 10 μm apart. The lack of cells in the first four annuli indicate the presence of an exclusion zone. B: density recovery profile (DRP). Each bar in the histogram shows the density of points in the corresponding annulus of the autocorrelation plot. The horizontal line indicates the mean density of points (166 cells/mm^2) and the vertical line (at 38 μm) shows the effective radius (see text). C: The L function is the scaled integral of the DRP. Solid line indicates the L function for the mosaic; dotted line indicates the curve that would be expected if the points were arranged randomly.

12.2.3 Boundary effects

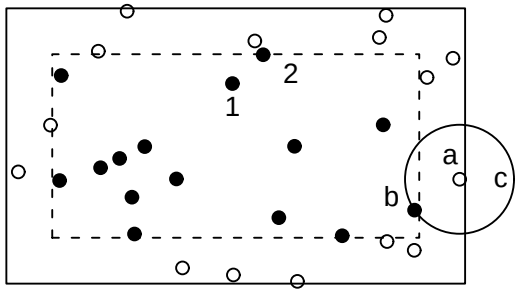

Fig. 12.6 Demonstration of boundary effects. The solid rectangle indicates the boundary region under study, with a central safety zone shown as dotted lines. Individual points (1, 2, a, b and c) are referred to in the text.

Figure 12.6 demonstrates the problems associated with boundary effects when quantifying retinal mosaics. For example, when finding the nearest neighbours, for cells in the centre of the region (e.g. cell 1) it is clear which cell is the nearest neighbour (cell 2). However, for a cell close to the boundary, such as cell a, although cell b is the closest within the field, there might have been another cell just to the right of the field that was closer to cell a (e.g. at point c or anywhere within the circle outside the field). Hence the estimate of the nearest neighbour for cells at the border is unreliable. To determine which cells are located at the border, we can add a 'safety zone', marked by the dotted line, and consider only the nearest-neighbour distances for neurons within the safety zone (filled symbols). However, what size of safety zone should be imposed? The larger the safety zone around the edge of the field, the smaller the impact of boundary cells. With larger safety zones however, fewer neurons are left within the safety region, and hence fewer samples to estimate the RI.

Imposing a safety zone is therefore simple, but requires another parameter (the width of the safety zone) and often discards a lot of data. Another technique for identifying border cells is to use the Voronoi tessellation, and label neurons as being at the border if their Voronoi polygon intersects with the field boundary. However, a subtler approach to handling boundary effects is to use weighting factors such that a contribution of e.g. each nearest-neighbour distance is measured, but the distances are weighted according to how close a neuron is to the border. One such edge-correction technique is to measure the fraction of the circumference of a circle (e.g. shown for point a in Figure 12.6) that lies within the field (Ripley, 1976; Diggle, 2002). This edge-correction term accounts for the $w(i, j)$ term in equation 12.1.

Another concern with boundary procedures that is often overlooked is the size of the field itself. Often, retinal mosaics are described simply by the x,y locations of each neuron — the coordinates of the (usually rectangular) field which determine which neurons are recorded are often not kept. As seen above, the position of the boundary is important, and affects the reliability of the measures taken from the mosaic. In the absence of a reported boundary region, one can be estimated by using

the extreme x and y coordinates of all the neurons. This is the smallest possible field, and although it is the maximum likelihood estimate (Ripley and Rasson, 1977), it is obviously an underestimate.

Ideally therefore, the field is decided in advance, placed onto the retinal tissue, and the positions of all neurons within that field should be recorded. What size should the field be? For practical purposes, most software assumes rectangular region (although some, such as SPLANCS (Rowlingson and Diggle, 1993) can handle arbitrary closed polygons). It should also be large enough to contain enough cells (e.g. at least 50), but small enough so that long-range spatial variations in density can be ignored. Again, some methodologies exist for handling non-homogeneities in spatial density across the field (Baddeley and Turner, 2005). However, often the long-range density variations observed across the retinal surface mean that investigators do not use very large fields, typically smaller than 1 mm $\times$ 1 mm.

12.3 Phenomenological approaches to modelling

What are the mechanisms underlying the development of these retinal mosaics? Progenitors of retinal neurons divide at the location of the photoreceptor layer, and once the neurons become postmitotic (i.e. stop dividing), they migrate through the retina to the appropriate layer for a given cell type. Certain cell types then migrate laterally within a layer to reach their final position (Reese and Galli-Resta, 2002). As well as these migratory processes, many other developmental mechanisms are thought to be involved, including lateral inhibition of cell fate and cell death (Reese and Galli-Resta, 2002). For a general review of the developmental mechanisms, see Cook and Chalupa (2000).

In addition to experimental approaches to understanding mosaic formation, theoretical modelling can help us evaluate the potential of different developmental mechanisms for generating such regular patterns. In this chapter I compare two styles of modelling:

phenomenological the focus is on generating model output that looks similar to observed data, using mechanisms that may or may not be biologically plausible.

mechanistic the primary concern is on modelling the cellular processes thought to be involved, rather than focusing on model output.

These two approaches are common in areas of biological modelling (e.g. see Nathan and Muller-Landau (2000)). In this section, I describe the phenomenological approaches; mechanistic approaches are discussed in the following section.

12.3.1 Exclusion zone models

The exclusion zone model is fairly straightforward and simply embodies the local rule that no two neurons should come closer to each other than some minimal distance. This local exclusion zone should then be able to recreate the hole seen in autocorrelation plots. This style of model was first applied to retinal mosaics by Shapiro et al (1985), who examined the spatial distribution of blue cone photoreceptors in macaque retinas. However, the exclusion zone model has been popularised by the more recent work of Galli-Resta and colleagues (Galli-Resta et al, 1997), where the model is termed the d_{min} model, where d_{min} is the main parameter of the model, representing the diameter of the exclusion zone. The value of d_{min} is normally not fixed, but drawn from a normal distribution with a given mean and standard deviation. The other parameters of the model (the field size and the number of cells) are taken from the observed mosaic being modelled.

The d_{min} model is an example of a serial model, where neurons are positioned one-by-one into the field (Figure 12.7). The starting point therefore is an empty field, the same size as the mosaic being modelled. A trial point is selected at random within the field, and a value for d_{min} is sampled from the normal distribution. If the nearest-neighbouring neuron in the field is closer than d_{min}, the trial cell is rejected, otherwise the trial cell is added into the field. This process continues until either the desired number of neurons have been added into the field or until it is no longer possible to fit any more neurons.

Once a field has been simulated using the d_{min} model, it can be compared against the observed mosaic (Figure 12.8). Visual comparisons are often inadequate, and so we use the quantitative methods (outlined in Section 12.2) to compare observed with simulated mosaics. We take advantage of the fact that we can generate many instances of simulated mosaics to estimate the goodness of fit. For example, if we use the RI as the metric to quantify regularity, we calculate the RI of the observed mosaic and the RI of each of 99 simulated mosaics from the d_{min} model (fixing the parameter values, and just varying the random number generator for positioning neurons). Informally, for a good fit, the RI of the observed mosaic should fall within the range of RIs generated by the d_{min} model.

This assessment of goodness of fit can then be quantified by calculating an empirical p value. If the RI of the observed mosaic is x_1 and the RI of $n-1$ simulated mosaics are $x_2 \ldots x_n$, then for each mosaic i we calculate a u_i value which determines the difference between the RI for mosaic i and the average RI of all other mosaics:

$$u_i = \text{abs}\left(x_i - \frac{1}{n-1}\sum_{j \neq i} x_j\right)$$

The expectation then is that if the model is a good fit to the data, u_1 should be of similar magnitude to all other u scores. A p value can then be calculated by sorting the values of u, largest first, and then counting the position of u_1 and dividing by n. For example, if u_1 was the ninth largest value of u out of 100, the p value would be

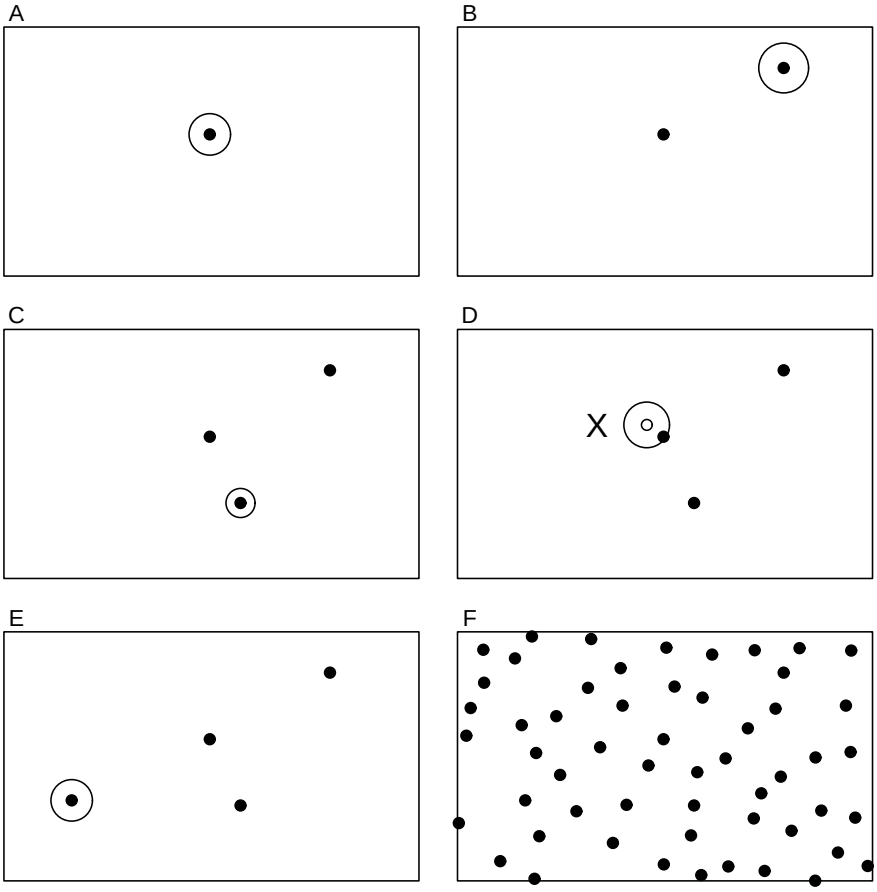

Fig. 12.7 Generation of a simulated mosaic using the d_{min} exclusion zone. In each panel, the rectangle shows the field with the trial cell surrounded by a circular exclusion zone. If no other cell is positioned within the exclusion zone, the trial cell is accepted into the field (panel D shows a trial cell being rejected). Panel A shows the starting condition: since there are no previous cells, the first trial cell is always accepted. Panel F shows the final mosaic after the desired number of cells have been added.

0.09. In this context, small p values indicates a poor fit of the model to the data, and the better the fit, the larger the p value. (Hence this test is one-tailed, and the model does not fit the data if $p \leq 0.05$ at the 5% significance level.) This procedure is rather general and can be adopted for other regularity measures, even for measures which are functions of distance, such as the L function; see (Diggle, 1986) for details.

This model assessment procedure is demonstrated in Figure 12.8. Three different parameter values for the d_{min} normal distribution are compared to see how well they can replicate an example mosaic (shown in panel A). Out of the three models, model 2 shows the best fit of simulated regularity indexes to the observed regu-

larity index. This is confirmed by computing the u scores and p values. Clearly, quantitative methods are required for comparing observed data and model output, as there are no strong visual differences among the three alternative models shown in Figure 12.8B–D.

Finally, Figure 12.9 shows the p values obtained by this procedure for a range of different model parameters. As the d_{min} model is relatively fast, such exhaustive parameter searches are feasible, and can easily pinpoint parts of parameter space where the model fits the data. For more complex models, an exhaustive approach is not feasible, and instead a heuristic search procedure should be used. Some other phenomenological models from the spatial statistics literature have specialised fitting procedures – for example see the R package SPATSTAT for details (Baddeley and Turner, 2005).

Evaluation of d_{min} model

The d_{min} model has been used to fit a wide range of mosaics of different cell types and different species (Galli-Resta et al, 1997, 1999; Cellerino et al, 2000; Raven et al, 2003). This strongly suggests that a homotypic exclusion zone is *sufficient* to generate a retinal mosaic. (In this context, *homotypic* means that interactions are restricted to cells of the same type; *heterotypic* interactions involve cells of different types.) This means it is unlikely that long-range interactions are required between cells of the same type, nor are interactions needed between cells of different types, confirming results from cross-correlation analysis (Rockhill et al, 2000; Mack, 2007). However, the d_{min} model does not say anything about the biological mechanisms underlying the generation of such local exclusion zones. I return to this topic in section 12.4.

12.3.2 Other phenomenological models

The d_{min} model is one instantiation of a whole class of phenomenological models whereby spatial points exhibit mutual exclusion (Diggle, 2002). A generalisation of this style of model is the pairwise interaction point process whereby a non-negative function $h(t)$ influences the probability of any two cells being a distance t apart. The shape of $h(t)$ can then determine both excitatory and inhibitory interactions between pairs of points, as demonstrated by Diggle (2002). These models also allow for a ‘birth-and-death’ style of cell positioning: cells are initially positioned randomly within the field, and then individual cells are killed and move to new positions. Such birth-and-death algorithms need several iterations to converge, but are preferable to the serial methods which may introduce order artifacts (cells added later into the field are more difficult to position than earlier-born cells). For further details see (Diggle, 2002; Eglen et al, 2005).

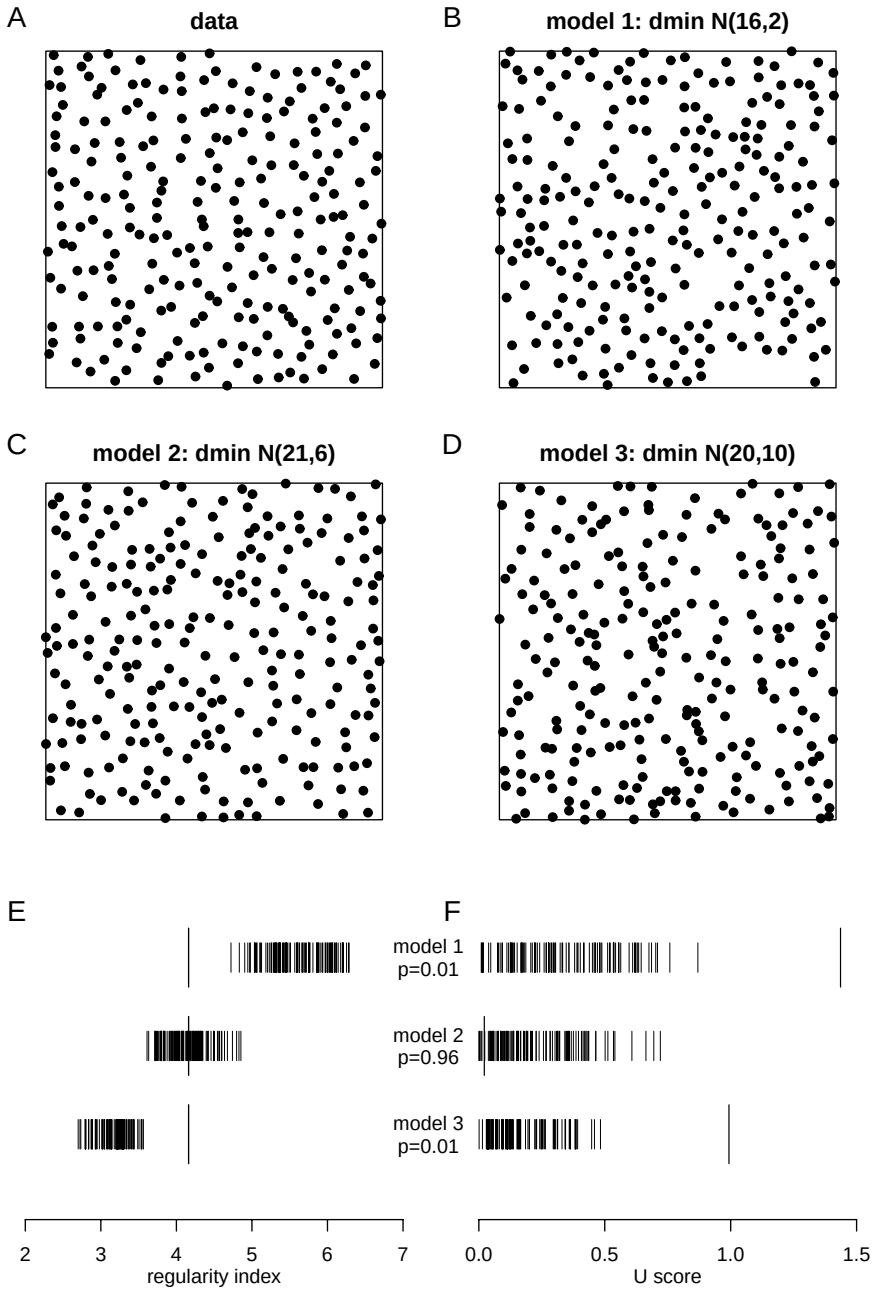

Fig. 12.8 Fitting the d_{min} model to an example mosaic. A: example observed mosaic (cholinergic amacrine cells in rat). The field of view is 400×400 μm^2. B–D: example simulations using three different values for d_{min} parameters; in each case the d_{min} value is drawn from a normal distribution with given mean and s.d. E–F: assessing the fit of each model to the data. In E, each row shows the regularity index from 99 simulations of each model; the larger vertical line in each case is the regularity of the observed data in A (4.16). Informally, the model fits the data if the observed RI falls within the range of the RIs generated by the model. Panel F shows the *u* score for each mosaic (real or simulated), with the score for the real mosaic drawn with a larger line. Whereas model 1 and 3 can be rejected, model 2 fits the data.

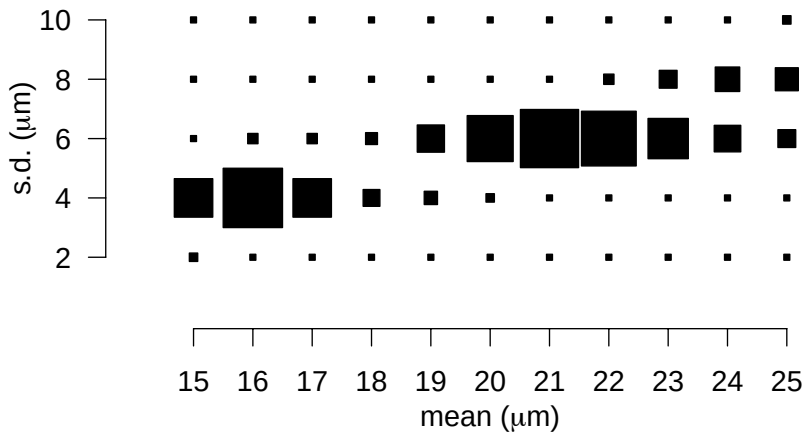

Fig. 12.9 Exhaustive parameter search of the d_{min} model to fit the observed mosaic shown in Figure 12.8A. For each value of the mean and s.d. of the d_{min} model, 99 simulations were generated, and the *p* value for comparing real and simulated mosaics obtained. The area of the square in each case is proportional to the *p* value.

Finally, in contrast to the models whereby local order emerges from random initial conditions, another class of model has been proposed for modelling retinal mosaics whereby an initially regular hexagonal mosaic is distorted to match the observed pattern. This 'distorted lattice' approach has been used to model the distribution of horizontal cells (Ammermüller et al, 1993) and retinal ganglion cells (Zhan and Troy, 2000). Although these models can recreate the spatial properties of observed retinal mosaics, they are of limited utility in informing us about the developmental mechanisms underlying mosaic generation as they require hexagonal mosaics to be first created and then distorted.

12.4 Mechanistic models

In this section I briefly discuss mechanistic models that have been proposed for generation of retinal mosaics. The key focus of these models is to help further understand the developmental mechanisms underlying pattern formation, as opposed to observing a good statistical fit between model and data. For further details of these models, the reader is referred to the original references and (Eglen, 2006).

12.4.1 Lateral migration

Once retinal neurons become postmitotic, they migrate radially through the layers of the retina until they arrive at the layer that is appropriate for their cell type. Whilst they migrate through the layers, it is thought that cells of the same type do not respect any minimal spacing rule (Galli-Resta et al, 1997). They therefore arrive randomly spaced over a period of several days. However, once they arrive in the destination layer, they appear to move laterally within the layer. The amount of lateral movement observed varies by cell type (Reese et al, 1999), and those that move more tend to have more regular mosaics.

What causes the lateral movement of neurons within their destination layer? Early evidence suggested a correlation between the time of movement and the first emergence of neurites in horizontal cells (Reese et al, 1999). This suggested that dendritic interactions might underlie the lateral migration, a hypothesis that was investigated using modelling techniques (Eglen et al, 2000), described in the next paragraph. Subsequently, further evidence for the role of dendritic interactions in mosaic formation came from work by Galli-Resta showing that temporary disruption of microtubules in dendrites caused mosaics to collapse; once microtubule function restored, mosaic organization returned (Galli-Resta et al, 2002). Most recently, mosaics are disrupted in mice lacking the cell adhesion molecule DSCAM, possibly as a consequence of altered dendritic fasciculation among homotypic neurons (Fuerst et al, 2008).

In the lateral migration model (Eglen et al, 2000), neurons initially have small circular dendritic arbors. Each cell receives input from its neighbours in proportion to the amount of dendritic overlap, and arbor size varies to maintain a fixed amount of input from neighbouring cells (van Ooyen and van Pelt, 1994). In addition, cells repel each other in proportion to their dendritic overlap. In this manner, as dendritic arbors develop, cells gradually begin to repel each other; once arbor sizes have stabilised, the cells then gradually settle into a regular hexagonal-like mosaic layout. The amounts that each cell moves is small, in line with the lateral distances observed experimentally (Reese et al, 1999). One limitation of the model is that it usually generates mosaics with regularity indexes that are much higher than those observed experimentally. This is because the model dendrites are perfectly circular and the amount of overlap between arbors is calculated exactly. Reducing the precision with which the amount of overlap is detected produces more realistic mosaics (Eglen et al, 2000). Subsequent modelling work has also examined in detail the mechanical forces that might compose the dendritic interactions, thus moving towards more realistic description of the developing dendrites (Ruggiero et al, 2004).

12.4.2 Lateral inhibition of cell fate

The eventual identity of any given neuron in the retina is not predetermined early in development but is influenced by many intrinsic and environmental factors during

development. Many cell fate mechanisms influence the identity of a given cell. One of the most common is lateral inhibition: neighbouring neurons compete to inhibit each other from acquiring a particular fate. There are many molecular pathways by which this lateral inhibition is mediated, but most notable is that of Delta-Notch signalling (Frankfort and Mardon, 2002). Cell fate mechanisms can therefore naturally impose minimal distance constraints as they prevent neighbours from being the same type of neuron.

The effect of cell fate interactions upon the relative numbers of primary and secondary fate neurons was studied by Honda et al (1990). This early modelling study showed that lateral inhibitory mechanisms are sufficient to generate the correct relative numbers of primary and secondary fate neurons in developing grasshopper neuroblasts. We have subsequently shown that lateral inhibition can generate regular primary fate mosaics from an initial irregular distribution of undifferentiated neurons (Eglen and Willshaw, 2002). However, if the initial population of undifferentiated neurons is already regular, the subsequent mosaic of primary fate neurons is not more regular than the initial population. Stochastic cell fate processes have also been shown theoretically to be sufficient to account for the generation of regular mosaics in zebrafish photoreceptors (Tohya et al, 1999). Further work by this group showed that these zebrafish mosaics could equivalently be generated by cell rearrangement processes (Mochizuki, 2002; Tohya et al, 2003).

12.4.3 Cell death

Many more neurons are produced in development than survive to adulthood. For example, estimates suggest that 50–90% of RGCS that are born will die before adulthood (Finlay and Pallas, 1989). This programmed cell death may have many roles in development, including the refinement of retinal projections to their targets (O'Leary et al, 1986). Cell death might be an active process in forming retinal mosaics, by removing those inappropriately-positioned neurons that are too close to their neighbours (Jeyarasasingam et al, 1998; Cook and Chalupa, 2000). The mechanisms by which neurons detect that they are too close too each other are however unknown. Furthermore, computer modelling of this process suggests that the cell death would need to be highly selective or the level of cell death would need to be very high to transform an irregular mosaic into a regular mosaic (Eglen and Willshaw, 2002). These modelling studies would therefore suggest that cell death alone does not account for the emergence of RGC mosaics (Jeyarasasingam et al, 1998). Cell death could however account for the generation of other mosaics, e.g. dopaminergic amacrine neurons (Raven et al, 2003), as the level of naturally-occurring cell death is very high and the final mosaics are only mildly regular.

12.4.4 Interactions between developmental mechanisms

Although cell death alone could not account for the emergence of RGC mosaics, it is likely that many mechanisms can co-operate to generate regular mosaics. Indeed, combining lateral inhibition of cell fate with cell death is sufficient to generate highly regular RGC-like mosaics (Eglen and Willshaw, 2002). The effects of interactions between several developmental mechanisms has been studied within the context of cellular patterns in the chick inner ear, the basilar papilla (Goodyear and Richardson, 1997), where primary fate cells are regularly distributed across the surface (Podgorski et al, 2007). Three different mechanisms were studied: lateral inhibition of cell fate, cell death, and differential adhesion. Individually, no single mechanism could account for the generation of the primary fate mosaics. However, iteratively coupling these mechanisms robustly generated regular patterns over a wide range of initial conditions. These results suggest that modelling the interactions between developmental mechanisms is clearly important before one can fully understand the relative role of individual processes, such as cell death.

12.5 Exclusion zone modelling: application to two types of neuron

This previous section has outlined several mechanisms that could underlie the generation of retinal mosaics, and in particular how an exclusion zone might be generated. If we assume that exclusion zones can somehow be generated, then it is natural to return to the d_{min} model and see how else it can be used to investigate mosaic formation. In particular, in this section we consider whether the d_{min} model can account for the generation of cellular patterns involving two related cell types.

Out of the 60+ cell types in the retina, there are several types of cell that come in complementary pairs (Cook and Chalupa, 2000). For example, the most prominent example of complementary pairing is the classification of alpha and beta RGCs into two types: on-centre or off-centre, depending on their response to light (Wässle et al, 1981a,b). Likewise, in both cat and macaque, horizontal cells are divided into two types, each regularly arranged (Wässle et al, 1978, 2000). In this section I show how exclusion zone modelling can test whether heterotypic developmental interactions are required to generate these mosaics.

Figure 12.10A shows the regular arrangement of two types of horizontal cell in macaque (Wässle et al, 2000). There are roughly twice as many type 1 neurons as type 2 neurons. The regularity index for all neurons (irrespective of type) is just under 4.0 (Figure 12.11), which is relatively high and thus lead to the suggestion that the two types of neuron might interact to create this high regularity (Wässle et al, 2000). To test this hypothesis, we extended the exclusion zone model to include two types of neurons (Eglen and Wong, 2008). Each neuron respected the exclusion zone only of cells of the same type; the only interaction between cells of different type

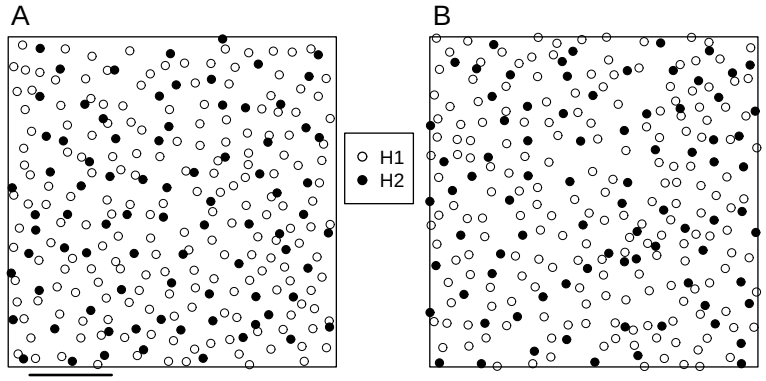

Fig. 12.10 Regular arrangement of two types of horizontal cells. A: observed distribution from macaque retina. Type 1 neurons are drawn as open circles, type 2 cells are filled. B: example output from the extended d_{min} model, assuming no interactions between cell types except for preventing somal overlap.

was that they could not come closer than about 12 μm, the average soma diameter, to prevent somal overlap. This model generated retinal mosaics that were both visually (Figure 12.10B) and quantitatively similar, as assessed by distribution of regularity indexes (Figure 12.11) and *L* functions (Eglen and Wong, 2008). Thus, the exclusion zone model predicts that horizontal cell mosaics can emerge without heterotypic interactions. A similar conclusion was reached for the generation of two types of beta RGCs in cat, using a more flexible exclusion zone technique (Eglen et al, 2005).

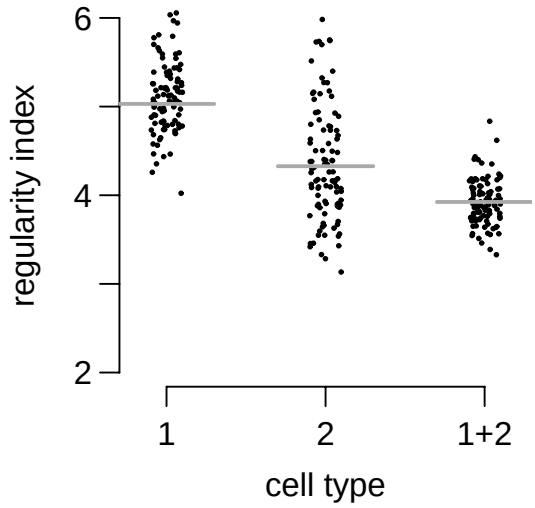

Fig. 12.11 Quantitative comparison of the extended d_{min} model with the macaque horizontal cells. The horizontal grey line shows the observed regularity index for either type 1 neurons, type 2 neurons, or all neurons, irrespective of type. Black dots indicate the regularity index from 99 simulations. The observed regularity index falls within the range of the 99 simulations, indicating a good fit between model and data.

12.6 Future directions

The retina is an ideal system for investigating questions of cellular patterning for several reasons. First, there is a comprehensive catalogue of individual retinal cell types (Masland, 2004), and although the number of cells seems large (60+), it is presumably much smaller than in other parts of the nervous system. Second, most cells of an individual type are located at a single depth within the retina, reducing the problem of cellular arrangements from three- to two-dimensions. Third, there are several selective neurochemical markers available to reliably stain individual cell types. (However, most of these markers only work reliably in adulthood, rather than early in development.) To see whether the principles of cellular organisation generalise from the retina to other parts of the central nervous system, several experimental challenges must be overcome. For example, we need reliable techniques for identifying and labelling individual cell types. Moving from two- to three-dimensional space will require accurate reconstruction within a volume (Oberlaender et al, 2009). By contrast, most of the theoretical techniques should generalise from the retina to other parts of the CNS (e.g. (Prodanov and Feirabend, 2007; Prodanov et al, 2007)) and into three dimensions (Baddeley et al, 1993). Most of the computational tools are also freely available in either Matlab or R (Rowlingson and Diggle, 1993; Baddeley and Turner, 2005; Eglen et al, 2008). Finally, aside from investigating developmental mechanisms, the analysis of spatial patterning of neurons in adulthood is also important in several clinical contexts (Diggle et al, 1991; Cotter et al, 2002; Lei et al, 2009). There has been relatively little modelling of spatial patterning in these clinical contexts, but as the technical limitations described above are overcome, I hope that computational modelling will be a useful tool in understanding the generation and perturbation of these patterns.

Acknowledgements This work was supported by funding from the Wellcome Trust and NIH. Experimental data kindly provided by Dr Lucia Galli-Resta and Prof Heinz Wässle. Thanks to Andreas Lønborg for comments on a draft version of this chapter.

12.7 Further Reading

- Statistical analysis of spatial point patterns (Diggle, 2002). This is a short but comprehensive description of most of the key techniques described in this chapter.
- Principles of computational modelling in neuroscience (Sterratt et al, 2011). Comprehensive textbook on modelling neural systems, including a chapter on neural development.
- Retinal development (Sernagor et al, 2006). Edited collection of articles describing the different stages of vertebrate retinal development.

References

Ammermüller J, Möckel W, Rugan P (1993) A geometrical description of horizontal cell networks in the turtle retina. Brain Research 616:351–356

Baddeley A, Turner R (2005) Spatstat: an R package for analyzing spatial point patterns. J Stat Software 12:1–42

Baddeley AJ, Moyeed RA, Howard CV, Boyde A (1993) Analysis of a three-dimensional point pattern with replication. Appl Stats 42:641–668, DOI 10.2307/2986181

Cellerino A, Novelli E, Galli-Resta L (2000) Retinal ganglion cells with NADPH-diaphorase activity in the chick form a regular mosaic with a strong dorsoventral asymmetry that can be modelled by a minimal spacing rule. European Journal of Neuroscience 12:613–620

Cook JE (1996) Spatial properties of retinal mosaics: an empirical evaluation of some existing measures. Visual Neuroscience 13:15–30

Cook JE (1998) Getting to grips with neuronal diversity. In: Chaulpa LM, Finlay BL (eds) Development and organization of the retina, Plenum Press, pp 91–120

Cook JE, Chalupa LM (2000) Retinal mosaics: new insights into an old concept. Trends in Neuroscience 23:26–34

Cotter D, Mackay D, Chana G, Beasley C, Landau S, Everall I (2002) Reduced neuronal size and glial cell density in area 9 of the dorsolateral prefrontal cortex in subjects with major depressive disorder. Cereb Cortex 12:386–394

Diggle P, Lange N, Benes F (1991) Analysis of variance for replicated spatial point patterns in clinical neuroanatomy. Journal of the American Statistical Association 86:618–625

Diggle PJ (1986) Displaced amacrine cells in the retina of a rabbit: analysis of a bivariate spatial point pattern. J Neurosci Methods 18:115–125

Diggle PJ (2002) Statistical analysis of spatial point patterns, 2nd edn. London: Edward Arnold

Eglen SJ (2006) Development of regular cellular spacing in the retina: theoretical models. Math Med Biol 23:79–99

Eglen SJ, Willshaw DJ (2002) Influence of cell fate mechanisms upon retinal mosaic formation: a modelling study. Development 129:5399–5408

Eglen SJ, Wong JCT (2008) Spatial constraints underlying the retinal mosaics of two types of horizontal cells in cat and macaque. Visual Neuroscience 25:209–214

Eglen SJ, van Ooyen A, Willshaw DJ (2000) Lateral cell movement driven by dendritic interactions is sufficient to form retinal mosaics. Network: Computation in Neural Systems 11:103–118

Eglen SJ, Diggle PJ, Troy JB (2005) Homotypic constraints dominate positioning of on- and off-centre beta retinal ganglion cells. Visual Neuroscience 22:859–871

Eglen SJ, Lofgreen DD, Raven MA, Reese BE (2008) Analysis of spatial relationships in three dimensions: tools for the study of nerve cell patterning. BMC Neuroscience 9:68

Finlay BL, Pallas SL (1989) Control of cell number in the developing mammalian visual system. Prog Neurobiol 32:207–234

Frankfort BJ, Mardon G (2002) R8 development in the drosophila eye: a paradigm for neural selection and differentiation. Development 129:1295–1306

Fuerst PG, Koizumi A, Masland RH, Burgess RW (2008) Neurite arborization and mosaic spacing in the mouse retina require DSCAM. Nature 451:470–474

Galli-Resta L (2002) Putting neurons in the right places: local interactions in the genesis of retinal architecture. Trends in Neuroscience 25:638–643

Galli-Resta L, Resta G, Tan SS, Reese BE (1997) Mosaics of Islet-1-expressing amacrine cells assembled by short-range cellular interactions. Journal of Neuroscience 17:7831–7838

Galli-Resta L, Novelli E, Kryger Z, Jacobs GH, Reese BE (1999) Modelling the mosaic organization of rod and cone photoreceptors with a minimal-spacing rule. European Journal of Neuroscience 11:1461–1469

Galli-Resta L, Novelli E, Viegi A (2002) Dynamic microtubule-dependent interactions position homotypic neurones in regular monolayered arrays during retinal development. Development 129:3803–3814

Goodyear R, Richardson G (1997) Pattern formation in the basilar papilla: evidence for cell rearrangement. Journal of Neuroscience 17:6289–6301

Hofer H, Carroll J, Neitz J, Neitz M, Williams DR (2005) Organization of the human trichromatic cone mosaic. Journal of Neuroscience 25:9669–9679

Honda H, Tanemura M, Yoshida A (1990) Estimation of neuroblast numbers in insect neurogenesis using the lateral inhibition hypothesis of cell differentiation. Development 110:1349–1352

Jeyarasasingam G, Snider CJ, Ratto GM, Chalupa LM (1998) Activity-regulated cell death contributes to the formation of on and off alpha ganglion cell mosaics. Journal of Comparative Neurology 394:335–343

Lei Y, Garrahan N, Hermann B, Fautsch M, Hernandez MR, Boulton M, Morgan JE (2009) Topography of neuron loss in the retinal ganglion cell layer in human glaucoma. Br J Ophthalmol 93:1676–1679, DOI 10.1136/bjo.2009.159210

Mack AF (2007) Evidence for a columnar organization of cones, Müller cells, and neurons in the retina of a cichlid fish. Neuroscience 144:1004–1014

Masland RH (2004) Neuronal cell types. Curr Biol 14:R497–R500, DOI 10.1016/j.cub.2004.06.035

Mochizuki A (2002) Pattern formation of cone mosaic in the zebrafish retina: a cell rearrangement model. Journal of Theoretical Biology 215:345–361

Nathan R, Muller-Landau HC (2000) Spatial patterns of seed dispersal, their determinants and consequences for recruitment. Trends Ecol Evol 15:278–285

Oberlaender M, Dercksen VJ, Egger R, Gensel M, Sakmann B, Hege HC (2009) Automated three-dimensional detection and counting of neuron somata. J Neurosci Methods 180:147–160

O'Leary DDM, Fawcett JW, Cowan WM (1986) Topographic targeting errors in the retinocollicular projection and their elimination by ganglion cell death. Journal of Neuroscience 6:3692–3705

van Ooyen A, van Pelt J (1994) Activity-dependent outgrowth of neurons and overshoot phenomena in developing neural networks. Journal of Theoretical Biology 167:27–43

Podgorski GJ, Bansal M, Flann NS (2007) Regular mosaic pattern development: A study of the interplay between lateral inhibition, apoptosis and differential adhesion. Theor Biol Med Model 4:43

Prodanov D, Feirabend HKP (2007) Morphometric analysis of the fiber populations of the rat sciatic nerve, its spinal roots, and its major branches. J Comp Neurol 503:85–100, DOI 10.1002/cne.21375

Prodanov D, Nagelkerke N, Marani E (2007) Spatial clustering analysis in neuroanatomy: applications of different approaches to motor nerve fiber distribution. J Neurosci Methods 160:93–108, DOI 10.1016/j.jneumeth.2006.08.017

Raven MA, Eglen SJ, Ohab JJ, Reese BE (2003) Determinants of the exclusion zone in dopaminergic amacrine cell mosaics. Journal of Comparative Neurology 461:123–136

Reese BE, Galli-Resta L (2002) The role of tangential dispersion in retinal mosaic formation. Progress in Retinal and Eye Research 21:153–168

Reese BE, Necessary BD, Tam PPL, Faulkner-Jones B, Tan SS (1999) Clonal expansion and cell dispersion in the developing mouse retina. European Journal of Neuroscience 11:2965–2978

Ripley B, Rasson J (1977) Finding the edge of a Poisson forest. J App Prob 14:483–491

Ripley BD (1976) The second-order analysis of stationary point processes. J App Prob 13:255–266

Rockhill RL, Euler T, Masland RH (2000) Spatial order within but not between types of retinal neurons. Proceedings of the National Academy Of Sciences of the USA 97:2303–2307

Rodieck RW (1991) The density recovery profile: a method for the analysis of points in the plane applicable to retinal studies. Visual Neuroscience 6:95–111

Roorda A, Metha AB, Lennie P, Williams DR (2001) Packing arrangement of the three cone classes in primate retina. Vision Research 41:1291–1306

Rowlingson BS, Diggle PJ (1993) SPLANCS: spatial point pattern analysis code in S-Plus. Comput Geosci 19:627–655

Ruggiero C, Benvenuti S, Borchi S, Giacomini M (2004) Mathematical model of retinal mosaic formation. Biosystems 76:113–120

Sernagor E, Eglen SJ, Harris WA, Wong ROL (eds) (2006) Retinal Development. Cambridge University Press

Shapiro MB, Schein SJ, deMonasterio FM (1985) Regularity and structure of the spatial pattern of blue cones of macaque retina. Journal of the American Statistical Association 80:803–812

Sterratt D, Graham B, Gillies A, Willshaw D (2011) Principles of computational modelling in neuroscience. Cambridge University Press

Tohya S, Mochizuki A, Iwasa Y (1999) Formation of cone mosaic of zebrafish retina. Journal of Theoretical Biology 200:231–244

Tohya S, Mochizuki A, Iwasa Y (2003) Difference in the retinal cone mosaic pattern between zebrafish and medaka: cell-rearrangement model. Journal of Theoretical Biology 221:289–300

Wässle H (2004) Parallel processing in the mammalian retina. Nat Rev Neurosci 5:747–757, DOI 10.1038/nrn1497

Wässle H, Riemann HJ (1978) The mosaic of nerve cells in the mammalian retina. Proceedings of the Royal Society of London Series B 200:441–461

Wässle H, Peichl L, Boycott BB (1978) Topography of horizontal cells in the retina of the domestic cat. Proceedings of the Royal Society of London Series B 203:269–291

Wässle H, Boycott BB, Illing RB (1981a) Morphology and mosaic of on-beta and off-beta cells in the cat retina and some functional considerations. Proceedings of the Royal Society of London Series B 212:177–195

Wässle H, Peichl L, Boycott BB (1981b) Morphology and topography of on-alpha and off-alpha cells in the cat retina. Proceedings of the Royal Society of London Series B 212:157–175

Wässle H, Dacey DM, Haun T, Haverkamp S, Grünert U, Boycott BB (2000) The mosaic of horizontal cells in the macaque monkey retina: with a comment on biplexiform ganglion cells. Visual Neuroscience 17:591–608

Zhan XJ, Troy JB (2000) Modeling cat retinal beta-cell arrays. Visual Neuroscience 17:23–39

Index

d_{min} model, 10

autocorrelation, 6

boundary effects, 8

cell fate, 16
complete spatial randomness (CSR), 5

density recovery profile (DRP), 6

exclusion zone model, 10

horizontal cells, 1

lateral inhibition, 16

mechanistic models, 9

phenomenological models, 9
photoreceptors, 1

regularity index (RI), 5
retinal ganglion cells (RGCs), 1
retinal mosaic, 1

Voronoi tessellation, 8